European Polymer Journal 116 (2019) 453–462

Contents lists available at ScienceDirect

European Polymer Journal

journal homepage: www.elsevier.com/locate/europolj

Composite organic encapsulate film with epoxy and benzoxazine

Gazi A.K.M. Rafiqul Bari, Haekyoung Kim*

School of Materials Science & Engineering, Yeungnam University, Gyeongsan, Gyeongbuk 712-749, Republic of Korea

ARTICLE INFO

Keywords:
Organic electronic device
Flexibility
Encapsulation
Barrier film
Benzoxazine
Epoxy

ABSTRACT

Electronic devices based on organic materials readily degrade owing to moisture or oxygen. Encapsulation materials and films made of inorganic and organic materials have been studied to arrest degradation, and polymeric materials have become more desirable owing to their flexibility, transparency, and processability. In this study, polymeric composite films that are fabricated under atmospheric conditions are studied. The composite encapsulation films consist of a combination of bisphenol A phenoxy resin and epoxy resin (POL) and synthesized benzoxazine monomer (eugenol-based Eu-Bzo (EZ), bisphenol-S based BPS-SA-Bzo (PZ), and bisphenol-AF based BPAF-SA-Bzo (FZ)). The composite with benzoxazine exhibits superior barrier characteristics with a highly hydrophobic nature compared to POL. The composite film with 3% Eu-Bzo exhibits lower moisture permeation rate of 2.02 $g\,m^{-2}\,d^{-1}$ with 90% transparency in comparison to POL (3.65 $g\,m^{-2}\,d^{-1}$) and PET (4.25 $g\,m^{-2}\,d^{-1}$). The novel composition of epoxy and phenoxy resins along with benzoxazine is a potential candidate for fabricating barrier materials for flexible printed organic electronics.

1. Introduction

Technological advances have spurred the development of various types of remarkable organic electronic devices, such as solar cells, organic light-emitting diodes (OLEDs) lightings, displays, and sensors [1–4]. In everyday life, people are increasingly relying on such types of organic devices. The poor stability of these devices is the main drawback for self-delamination and degradation due to environmental factors such as moisture and oxygen. The degradation generally starts with the electrochemical reduction of water molecules at the organic/cathode interface [5,6]. Therefore, an encapsulation film is an essential component for safeguarding organic devices. Further, the barrier range usually depends on the application area. For example, the required water vapor transmission rate for an OLED is less than $10^{-6}\,g\,m^{-2}\,d^{-1}$ whereas that for an organic thin film transistor (TFT) is between 0.1 $g\,m^{-2}\,d^{-1}$ and 0.0001 $g\,m^{-2}\,d^{-1}$ [7].

Generally, various fabrication techniques are used to obtain well-formed barrier layers. An alternating organic–inorganic multi-layer is the currently preferred approach [8–11]. Inorganic materials usually provide better barrier function than organic materials [12,13], but have issues regarding flexibility, transparency, and processing approach [14–17]. Further, an inorganic layer embedded in an organic layer or substrate is difficult to maintain. As a consequence, the surface of the substrate needs to be modified [18,19]. This is why high-barrier organic films are needed for flexibility and ease of processing. In general, organic-based polymers are of two types, namely, thermosetting and thermoplastic polymers. Processing of thermoplastic polymers requires higher temperatures and complex processes, such as extrusion and blowing [20,21], whereas thermosetting polymers crosslink with each other with the aid of curing agents, and their melting cannot be reversed. Epoxy resin is an example of a thermosetting polymer that can vary with molecular weight for different epoxy equivalent weights; it can also achieve flexibility by incorporating various groups within the structure [22]. However, phenoxy resin is a very different type of polymer that has the combined properties of both thermoplastic and thermosetting polymers. Each molecular chain of the phenoxy resin contains a functional group that allows crosslinking. Phenoxy resin has excellent thermal and chemical resistances, low water percolation, and high adhesiveness. In addition to these excellent features, phenoxy resin has a small coefficient of linear thermal expansion; it has excellent transparency and can be used to fabricate flexible films [23]. Another example of a thermosetting polymer is polybenzoxazine, which is easily synthesized without the use of catalysts. Typically, thermosetting polymers undergo volumetric shrinkage after curing, whereas benzoxazine (Bzo) maintains geometrical stability. Benzoxazine does not release any toxic byproducts during curing and retains its property of low water absorption [24–27].

In this study, we synthesized a blend of two different types of resins: high-molecular-weight phenoxy resin (YP 50) and silane-modified epoxy resin (KSR 177). In addition, three different benzoxazine

* Corresponding author.
E-mail address: hkkim@ynu.ac.kr (H. Kim).

https://doi.org/10.1016/j.eurpolymj.2019.04.039
Received 30 January 2019; Received in revised form 17 April 2019; Accepted 21 April 2019

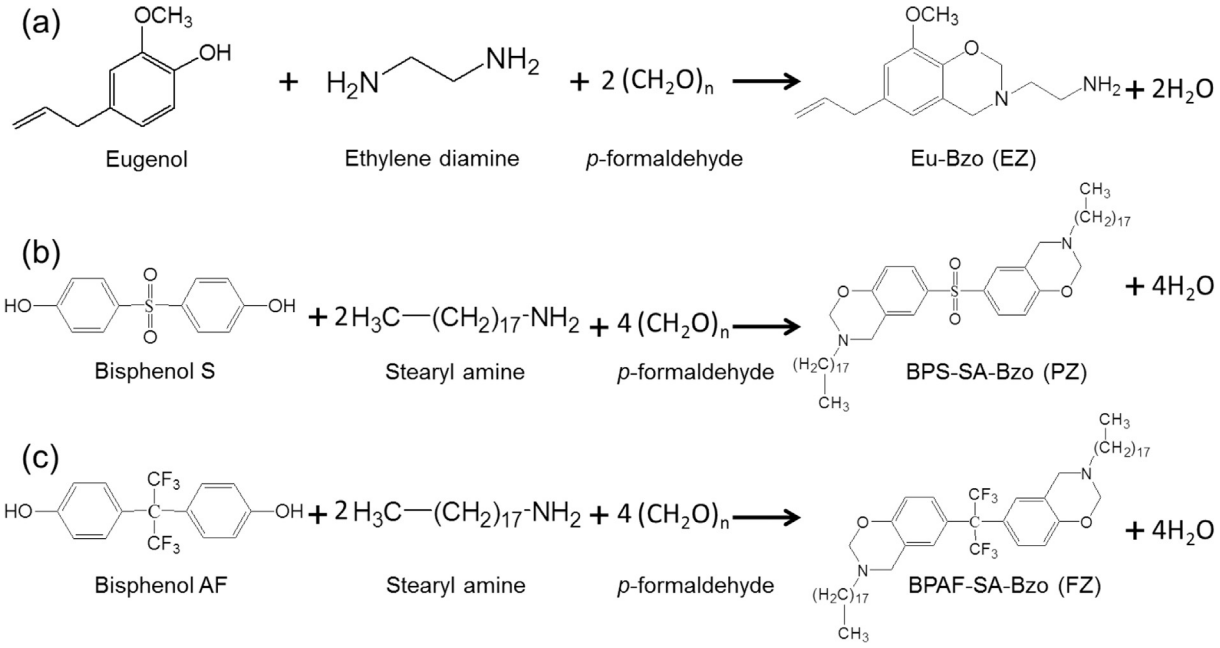

Scheme 1. Synthesis of Bzo monomers (a) Eu-Bzo (EZ), (b) BPS-SA-Bzo (PZ), and (c) BPAF-SA-Bzo (FZ).

monomers have been synthesized: eugenol-based eugenol benzoxazine (Eu-Bzo) (EZ), bisphenol-S-based bisphenol S stearyl amine benzoxazine (BPS-SA-Bzo) (PZ), and bisphenol-AF-based bisphenol AF stearyl amine benzoxazine (BPAF-SA-Bzo) (FZ) monomers (Scheme 1). These three monomers were blended with epoxy/phenoxy compositions separately to obtain composite polymer solutions. Films were then fabricated from these solutions under atmospheric conditions using an applicator with a bar coater.

2. Experimental

2.1. Materials

Epoxy resin (KSR 177) and phenoxy resin (YP 50) were purchased from Kukdo Chemical Co. Ltd. Imidazole, eugenol, ethylenediamine, *p*-formaldehyde, and dimethyl sulfoxide were purchased from Sigma-Aldrich. Stearyl amine and 4,4′-sulfonyldiphenol were purchased from Acros Organics. Methyl ethyl ketone (MEK) was obtained from Daesung Chemical Co. Ltd.

2.2. Synthesis of Bzo monomers

In a glass round-bottom flask equipped with a condenser, *p*-formaldehyde and DMSO (20 ml) were added and stirred continuously at 50 °C. Amine (ethylene diamine for Eu-Bzo and stearyl amine for BPS-SA-Bzo and BPAF-SA-Bzo) was added gradually to this solution. Meanwhile, phenolic derivatives (eugenol for Eu-Bzo, bisphenol S for BPS-SA-Bzo, and bisphenol AF for BPAF-SA-Bzo) with dimethyl sulfoxide (10 ml) solution were prepared separately. After fully adding the amine, the phenolic derivative solution was added to the mixture dropwise. The reaction temperature was maintained at 120 °C and the mixture was continuously stirred for 3 h, after which a pale yellow transparent solution was obtained. The solution was cooled to room temperature and precipitated in 1M NaOH solution. The obtained precipitate was filtered and washed with distilled water many times, and the precipitate was subsequently dried at 50 °C for 12 h [28,29]. The weights of the materials are as follows: Eu-Bzo - eugenol: 3.28 g, ethylenediamine: 1.34 g, *p*-formaldehyde: 1.8 g; BPS-SA-Bzo - bisphenol S: 2.5 g, stearyl amine: 5.39 g, *p*-formaldehyde, 1.8 g; BPAF-SA-Bzo - bisphenol AF: 3.36 g, stearyl amine: 5.39 g, *p*-formaldehyde: 1.8 g (Scheme 1); stoichiometric expression.

2.3. Processing of polymer solution (POL)

The reactor was set up in a fume hood. A four-necked lid was tightly clamped with a jacketed vessel, which was connected to an overhead digital high-speed stirrer, a circulator of hot water (temperature controlled), a water-cooled condenser, and nitrogen gas. The solution of epoxy (KSR 177) and MEK were prepared in a beaker at 50 °C. At 60 °C, MEK and phenoxy (YP 50) were stirred into the reactor until the mixture melted. Then, epoxy was added to the reactor and stirred continuously under a nitrogen environment. Finally, imidazole as a curing agent was added to the solution and stirred for an hour. The material ratio is as follows: KSR 177: 31.9%, YP 50: 21.6%, MEK: 46%, and Imidazole: 0.4%.

2.4. Polymer and Bzo composite solution processing

First, the POLs are filled in different vials. EZ, PZ, and FZ are separately filled in vials as well. Each of the monomers was previously dissolved in 1 g MEK solution separately to prepare the EZ, PZ, and FZ solutions. Then, these solutions are added individually to the prepared POL solutions separately. Finally, all the solutions are stirred at 50 °C till clear solutions are obtained. The solutions are now coded as POL, EZX, PZX, FZX, where X is the ratio of the Bzo monomer to POL, e.g., 1 wt% EZ to POL, 1 wt% PZ to POL, and 1 wt% FZ to POL are coded as EZ1, PZ1, and FZ1, respectively.

2.5. Film preparations

For the film fabrication, a 0.5-mm applicator gap was maintained to coat the polyethylene terephthalate (PET) substrate (rinsed with isopropyl alcohol and dried) with a bar coater using an applicator. Fig. 1 represents a schematic of the coating of the film. The coated films were dried at 50 °C for 12 h and heated at 120 °C for 1 h for further analysis (Scheme 2) [30,31]. The films were coded as a POL, EZX, PZX, and FZX in the same manner as before, where X is the ratio of the Bzo monomer to POL. Further, POL, EZX, PZX, and FZX without imidazole were coded as POL-IMI0, EZX-IMI0, PZX-IMI0, and FZX-IMI0, respectively.

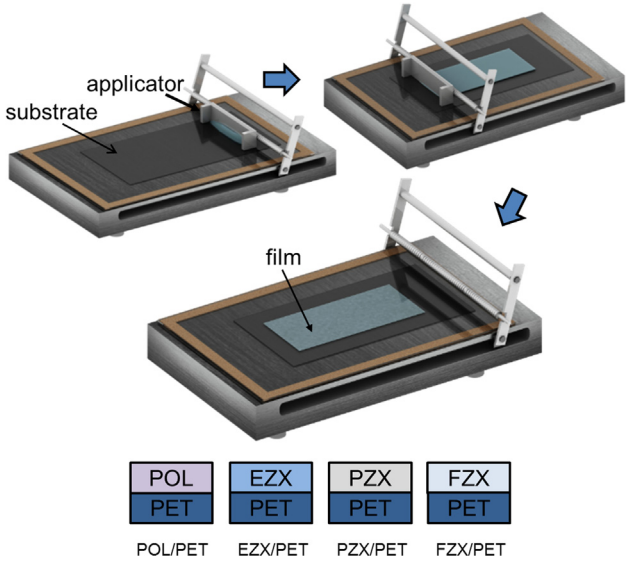

Fig. 1. Schematic of coating of barrier film on substrate using applicator.

2.6. Characterizations

The Fourier transform infrared (FTIR) spectra were obtained using the Nicolet 6700 spectrometer to confirm the structure of the benzoxazine. An FT-NMR VNS600 instrument was used to obtain the nuclear magnetic resonance (NMR) spectra for ^{1}H NMR and ^{13}C NMR. DMSO-d_6 was used as the solvent to dissolve the monomer. To confirm or study the completion of curing for films, a TA Instruments Q200 differential scanning calorimeter (DSC) was used (heating rate: 10 °C/min, N_2 flow rate: 50 ml/min). The transmittances of the films were obtained with the GENESYS™ 10S UV–Vis spectrophotometer. For the swelling measurements, the coated films were peeled from the PET substrate, cut into 20 mm × 20 mm sections, and placed in an oven for complete drying for 24 h at 50 °C. After cooling to the ambient temperature, the initial weights of the films were recorded. The films were then

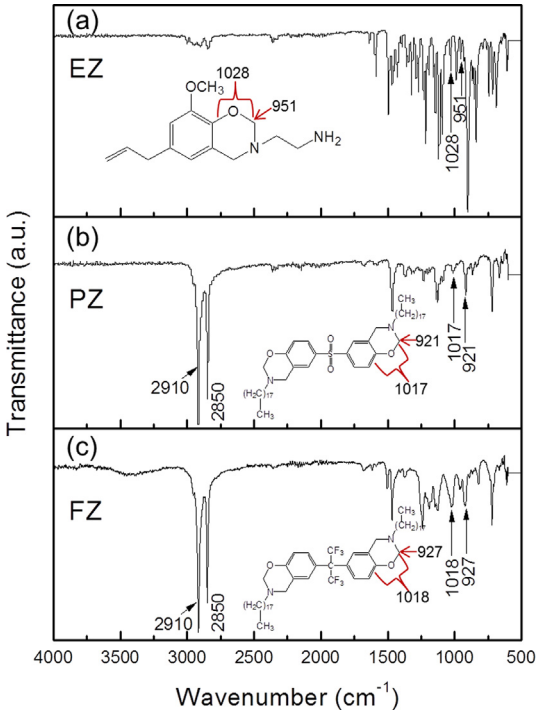

Fig. 2. FTIR spectra of (a) EZ, (b) PZ, and (c) FZ.

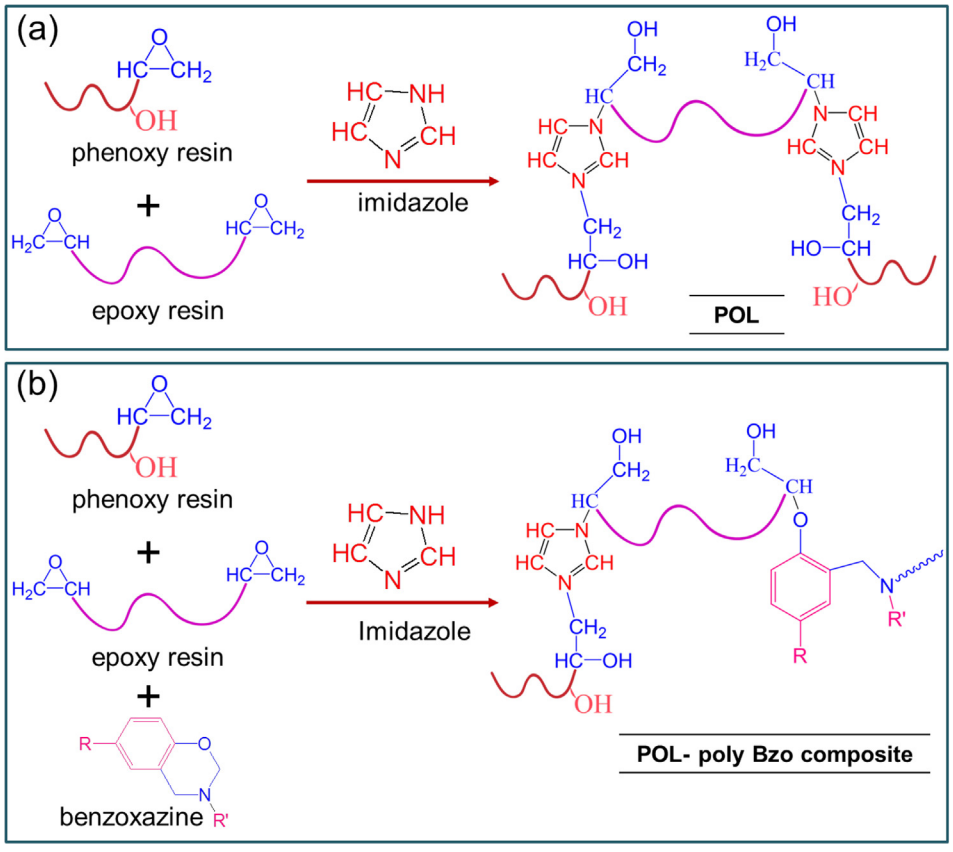

Scheme 2. Reaction mechanism of formation of (a) POL, and (b) POL-poly Bzo composite.

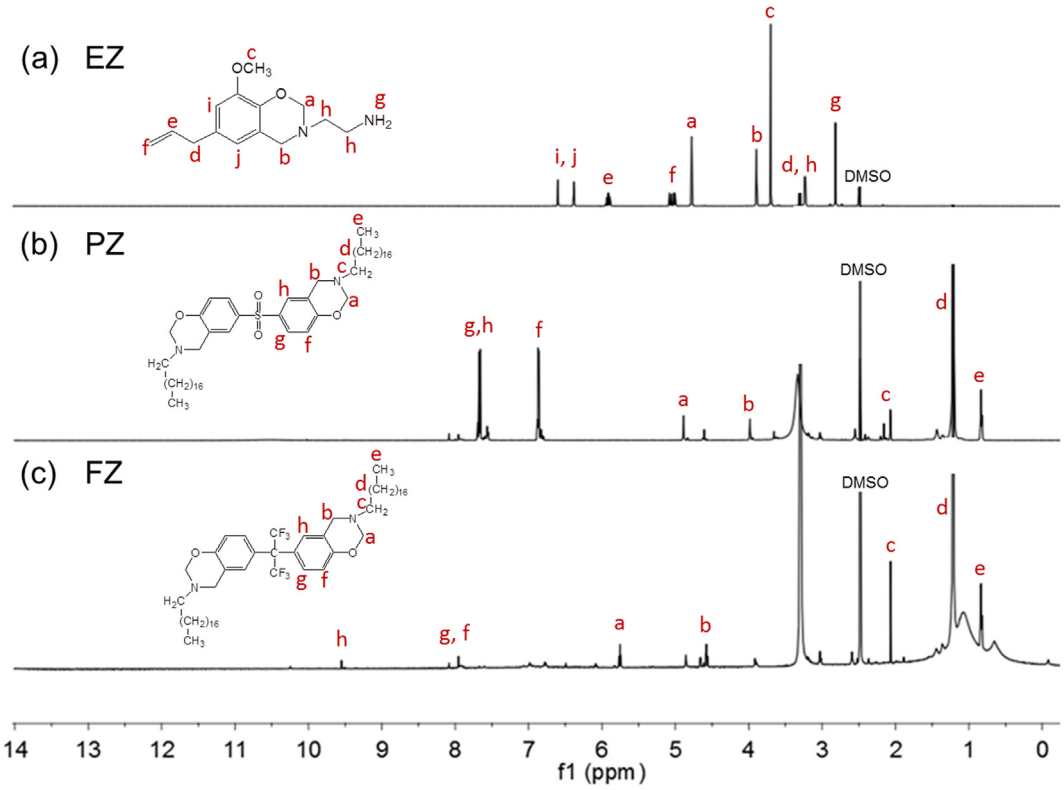

Fig. 3. ^{1}H NMR spectra of (a) EZ, (b) PZ, and (c) FZ.

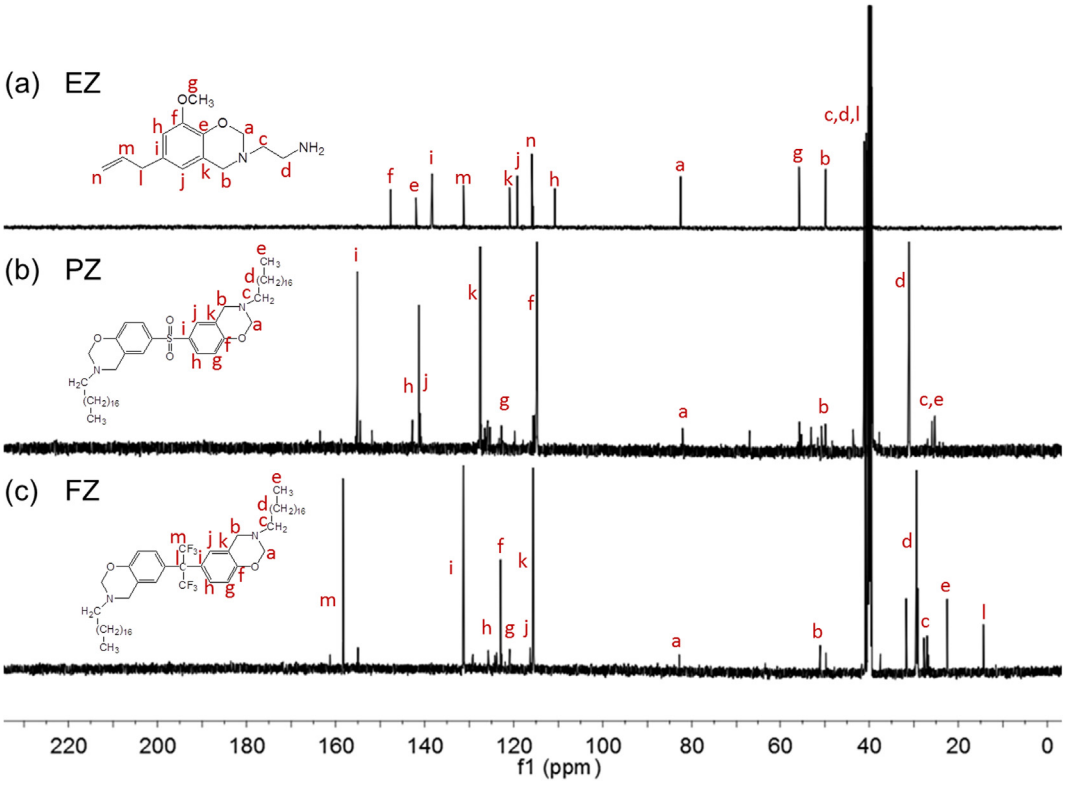

Fig. 4. ^{13}C NMR spectra of (a) EZ, (b) PZ, and (c) FZ.

submerged in de-ionized water for 24 h. Subsequently, the surface water on the films was removed carefully using a wiper. The final weights of the wet films were then measured, and the difference between the initial and final weight was calculated [32]. The contact angles of the films were measured using an OCA 20 data physics Germany CA analyzer by placing a water drop of 10 µl on the surface of each film using a micro syringe. An Instron 3345 model instrument was used to measure the mechanical properties of the films. The films were

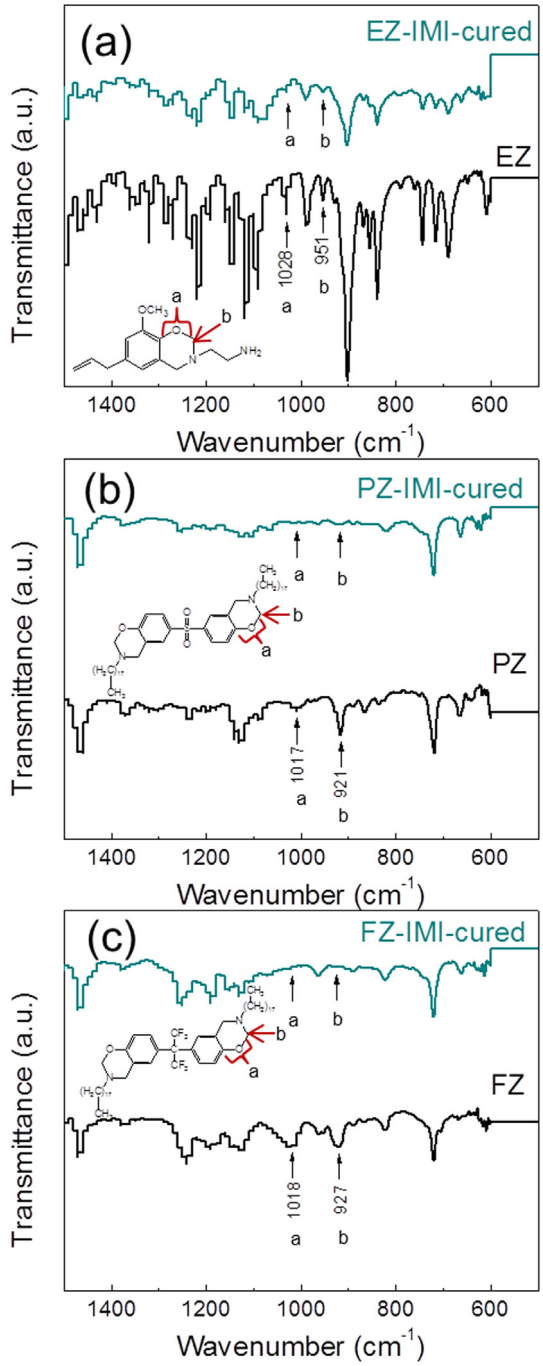

Fig. 5. FTIR spectra of monomer before/after cure at 120 °C for an hour with imidazole (a) Eu-Bzo (EZ), (b) BPS-SA-Bzo (PZ), and (c) BPAF-SA-Bzo (FZ).

cut into 100 mm × 30 mm sections. For the chemical resistance test, the films were peeled from the substrate and completely immersed in 1M HCl solution and 1M NaOH for 30 min. Then, the films were dried at 100 °C for 15 min. The weight differences before and after immersions were calculated [33]. For the measurement of the barrier abilities of the films, a lab-designed moisture permeation rate (MPR) measurement technique was used. The details of this measurement technique have been noted in a previous work [34].

3. Results and discussions

Fig. 2 shows the FTIR spectra of the Bzo monomers of EZ, PZ, and FZ. Typical Bzo ring vibrations were observed at 951 cm^{-1}, 921 cm^{-1}, and 927 cm^{-1}, and the symmetric stretching vibrations of C—O—C were seen at 1028 cm^{-1}, 1017 cm^{-1}, and 1018 cm^{-1} for EZ, PZ, and FZ, respectively [35–37]. The bands of the EZ monomer moved to a higher wavenumber compared to those of the PZ and FZ monomers. The electron-donating group of the EZ monomer increased the energy of the bending vibrations of the Bzo ring [38]. The strong vibration peaks at 2910 cm^{-1} and 2850 cm^{-1} for the PZ and FZ correspond to the stearyl amine $-CH_2$ stretching peak [39]. Fig. 3 shows the ^1H NMR spectra of the EZ, PZ, and FZ monomers. The characteristic two-protons of Ar-CH_2-N and O-CH_2-N (oxazine ring) are confirmed as singlets at 3.89 and 4.78 ppm for EZ, 3.98 and 4.89 ppm for PZ, and 4.58 and 5.75 ppm for FZ, respectively [35,37]. Fig. 4 depicts the ^{13}C NMR spectra for the three monomers. The oxazine ring characteristic resonance spectra appear at 82.5 and 49.7 ppm for EZ, 82.3 and 49.8 ppm for PZ, and 82.5 and 50.9 ppm for FZ, respectively, for the O-CH_2-N and Ar-CH_2-N [37]. In the case of PZ and FZ, there are some impurity peaks in the spectra. At the time of the synthesis of the monomers, the 1 M concentration of NaOH was retained. It is probable that some unreacted part of each monomer did not dissolve with this concentration and remained as is. Fig. 5 compares the FTIR spectra of the monomers with imidazole after heating at 120 °C for 1 h. The typical peaks of the Bzo ring and stretching vibrations of the C—O—C have disappeared, which indicate the opening of the oxazine ring and polymerization of the Bzo monomers. Fig. 6 compares the FTIR spectra of POL, EZ5, PZ5, and FZ5 after curing. The epoxy peaks of YP 50 and KSR 177 in the vicinity of 958 cm^{-1} have disappeared in the case of POL, EZ5, PZ5, and FZ5 (Fig. 6b). The epoxy group ring opening thus provides the OH group; thus, in the vicinity of 3500 cm^{-1}, the OH broadening is observed (Fig. 6a). This proves the epoxy group ring opening and polymerizations of POL, EZ5, PZ5, and FZ5.

To analyze the curing mechanism of polymers with respect to temperature, we performed the differential scanning calorimetry (DSC) of polymers and monomers under different conditions. DSC provides information on the transition of materials with heat flows [40]. Fig. 7 shows the DSC thermograph of polymers. Films without the imidazole, both non-heated and heated, do not exhibit an exothermic peak (Fig. 7a & b). It is proven that there is no transition of materials or crosslinking among polymers without imidazole. The addition of imidazole to the mixture results in exothermic peaks in the range of 147–151 °C (Fig. 7c). From this result, we can say that imidazole initiates crosslinking among epoxy and Bzo groups. Further, copolymerization between the poly Bzo phenolic group and the epoxy occurs after the formation of the poly Bzo [41,42]. Heated polymers with imidazole do not show an exothermic peak (Fig. 7d), which proves the completion of the polymerization. To further analyze Bzo-monomer polymerization behavior, we performed the DSC of the Bzo monomer without imidazole (Fig. 8a) and with imidazole (Fig. 8b). The onset transition temperature of the EZ, PZ, and FZ monomer were 204, 142, and 130 °C, respectively. The maximum temperature peaks of EZ, PZ, and FZ were 236, 173, and 154 °C, respectively. The highest rate of transition occurs for each monomer at this temperature [43]. Three different types of Bzo monomers have shown different transition temperatures. The methoxy group (OCH_3) of a phenolic derivative is an electron-donating group, and it is more favorable for the synthesis of the EZ monomer. Moreover, this electron-donating group increases the electron density at the oxazine ring; as a consequence, the monomer becomes relatively stable. Therefore, the EZ monomer requires a higher polymerization temperature (236 °C). On the contrary, the electron-withdrawing groups of PZ (O═S═O) and FZ (CF_3) decrease the charge density from the bisphenol. The charge density in O on the oxazine ring is also low, and it is easier to cleave to the initiating polymerization at a lower temperature [38]. When the imidazole is added to Bzo monomer, the onset of the exotherm reduces to 121, 121, and 105 °C for EZ, PZ, and FZ, respectively. The highest peaks of the exotherm are also reduced to 145, 155, and 150 °C for EZ, PZ, and FZ (Fig. 8b). It appears that imidazole acts as a catalyst or cross linker to reduce the polymerization

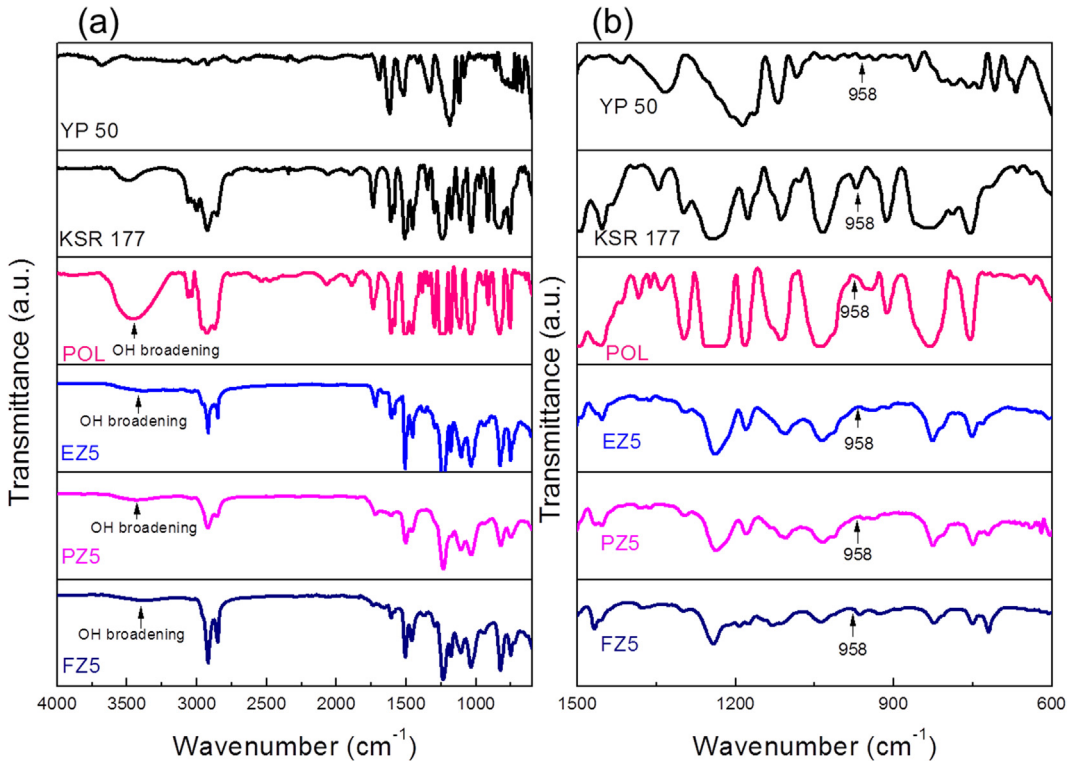

Fig. 6. FTIR spectra of POL, EZ5, PZ5, and FZ5 after cure at 120 °C for an hour with imidazole.

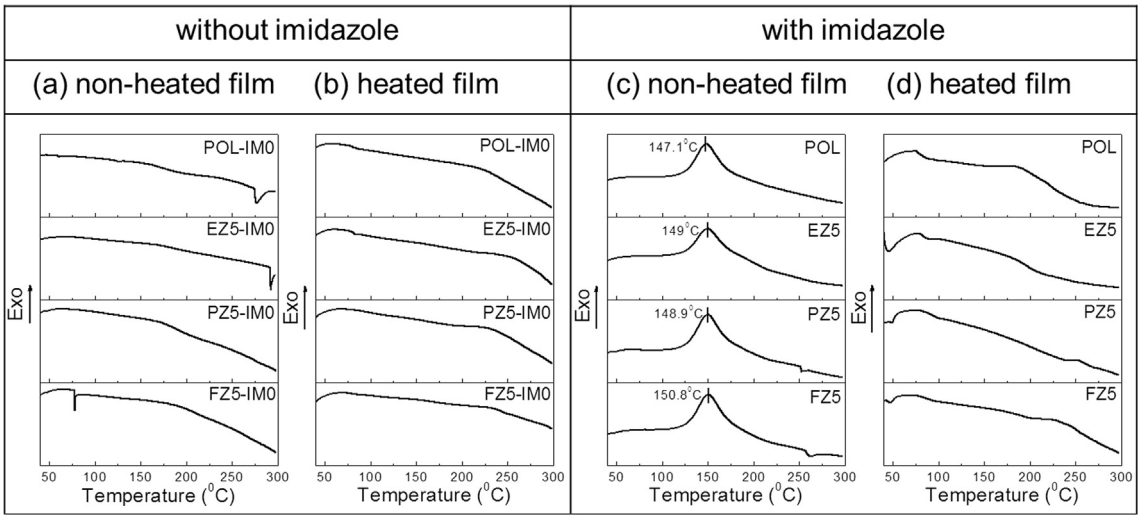

Fig. 7. DSC analysis of films (a) non-heated without imidazole, (b) heated without imidazole, (c) non-heated with imidazole, and (d) heated with imidazole.

temperature of the Bzo [44]. In general, imidazole is amphoteric, acting as both an acid and a base. Lewis acid is used as a catalyst for the curing of the Bzo group, which initiates the polymerization of the Bzo group [45]. As a consequence, for all Bzo groups, the polymerization temperature decreases with the addition of imidazole [46]. Fig. 9a represents the transparency of films, which is a very important factor for an organic electronic device, such as displays and solar cells [1,47]. POL/PET, EZ1/PET, EZ3/PET, EZ5/PET, and EZ7/PET films demonstrate excellent transparency (> 88% at 550 nm). The good distribution of the EZX to POL results in higher transparency for the EZX/PET films, which is shown in the optical microscopic image of Fig. 9d. In general, the higher degree of phase dispersions among polymers can yield good transparent materials [48,49]. For the EZ polymer, good dispersions on the polymer and a shorter length of ethylene amine with the crosslinked nitrogen atom resulted in high clarity of the EZ and epoxy composition film. On the contrary, the PZX/PET and FZX/PET films do not provide sufficient transparency (Fig. 9b & c). The agglomerate entanglement of the long chain of a stearyl group of PZ and FZ probably causes the low transparency. Fig. 9e show the thickness of the films. The thickness of the films changes with the ratio of the Bzo. The thickness of the POL is 0.148 mm. In every case, with the addition of Bzo, the thickness of the films reduced. The thickness of EZ3 was 0.128 mm and the PET substrate was 0.080 mm.

Fig. 10a shows the average contact angle of the films. The average contact angle for the POL film is 86.5°. The EZ3 film shows the lowest contact angle of 70.1°, and the FZ10 film exhibits the highest contact angle of 101.2° among the films. Fig. 10b shows the stress–strain outcome of the films. The POL film showed the 70.3 MPa tensile strengths. In every case, tensile strength increased by the addition of Bzo to POL. The tensile strength of EZ5, PZ5, and FZ5 were 89.4, 75.4, and

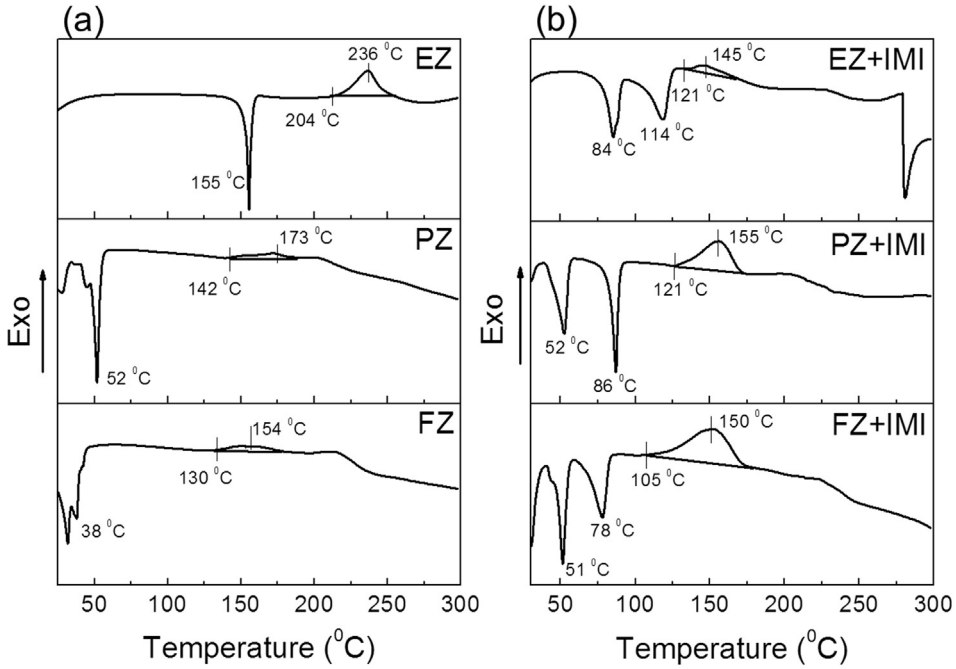

Fig. 8. DSC analysis of (a) Bzo monomers without imidazole, and (b) Bzo monomers with imidazole.

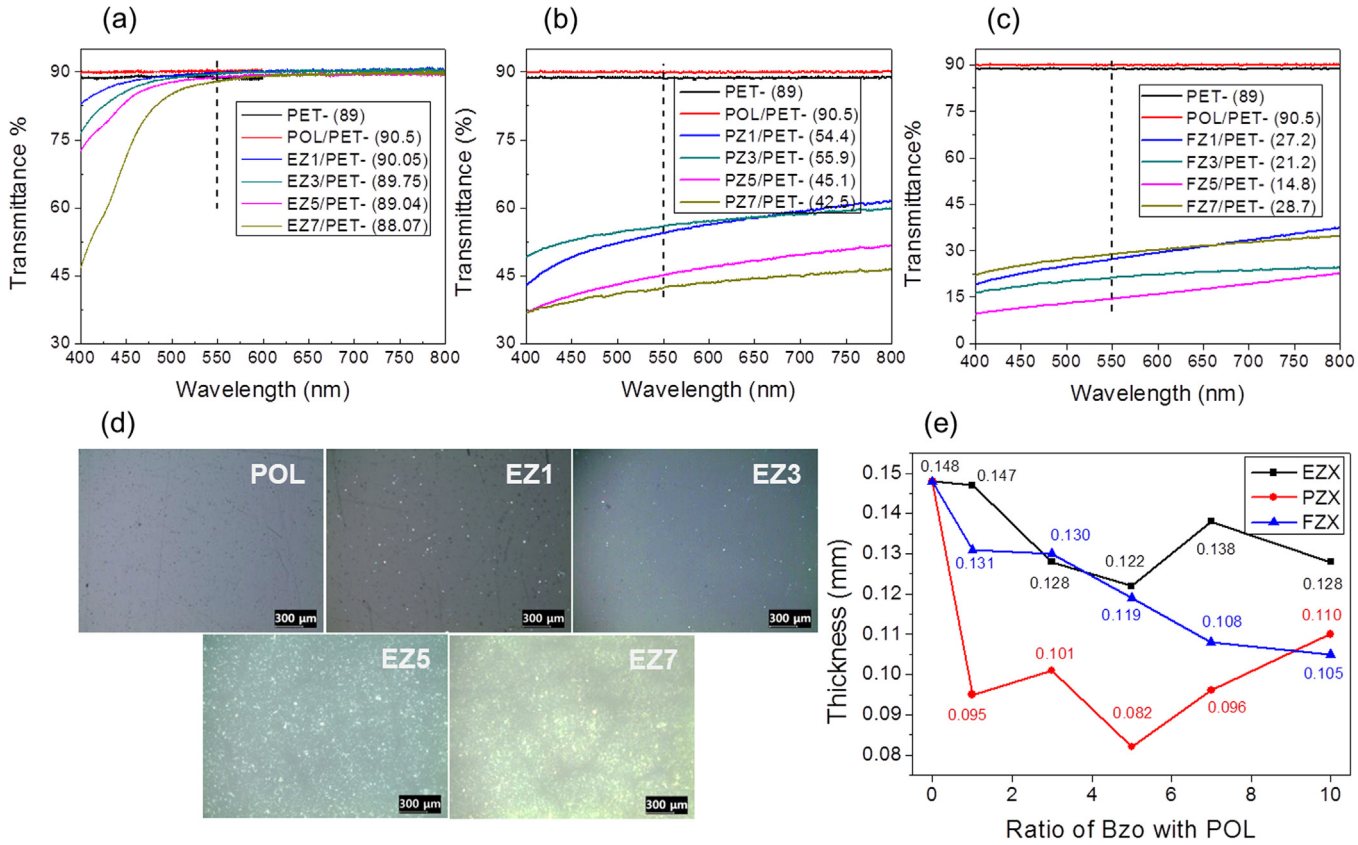

Fig. 9. Transmittance of (a) EZX/PET, (b) PZX/PET, (c) FZX/PET films, (d) optical microscope image of EZX films (×50 magnification), and (e) thickness of films.

72.1 MPa, respectively. The electrical behavior of the films has measured by the four-probe method. All the films exhibited nonconductive properties, which are an advantageous for barrier films.

The chemical resistance was measured to characterize the stability in corrosive environments. Films are susceptible to degradation by the effect of chemicals. The chemical resistance of films is shown in Fig. 11. The reduction in film weights are shown for 1 M HCl acid solutions and 1 M NaOH basic solutions. The addition of EZ to POL increases the stability of the films in acid and basic solutions. In an acidic medium, the films of PZ to POL up to 5% and the films of FZ to POL up to 3% are more stable than the POL film. In a basic medium, both PZ and FZ to POL up to 7% composite show more stability than the POL film. Among

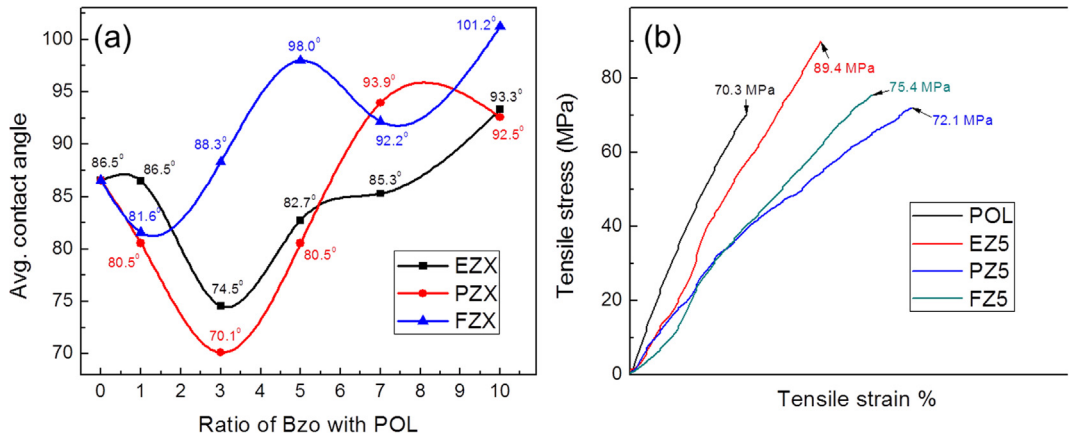

Fig. 10. (a) Avg. contact angle, and (b) stress-strain behavior of the films.

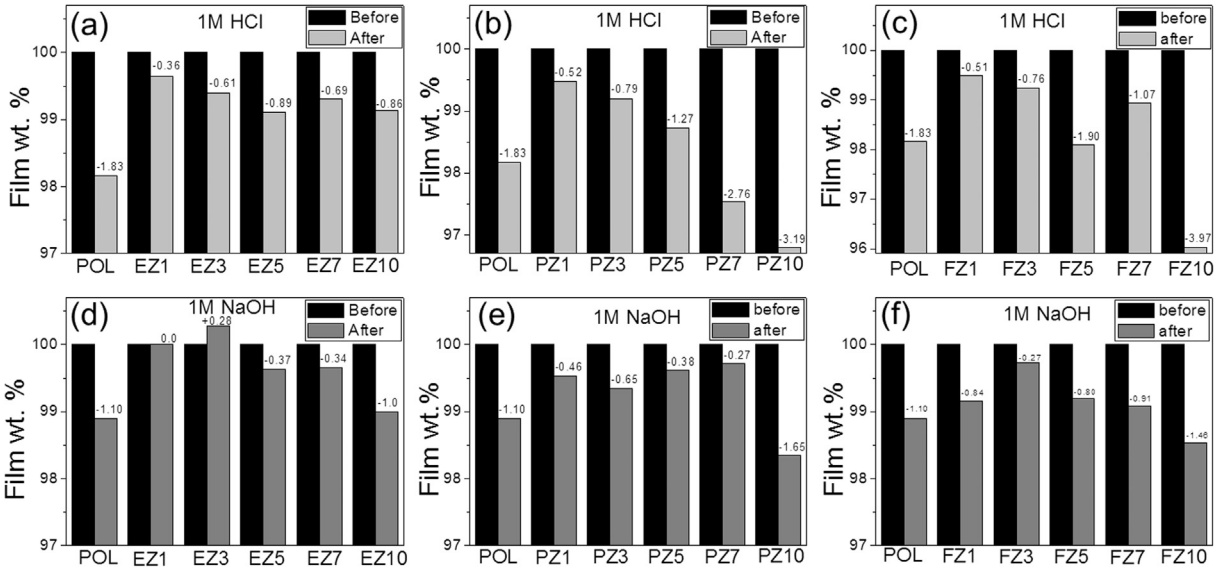

Fig. 11. Chemical resistance of (a) EZX in HCl, (b) PZX in HCl, (c) FZX in HCl, (d) EZX in NaOH, (e) PZX in NaOH, and (f) FZX in NaOH.

the Bzo groups, composite films with EZ show better stability than the POL film in both media for all ratios.

The water absorption properties of films are characterized by the swelling test, as shown in Fig. 12a. In all cases, the swelling decreased compared with POL when Bzo forms a composite with the POL. For all the ratios of three different Bzo films, EZ7 (0.94%), PZ7 (0.57%), and FZ10 (0.37%) show the lowest swelling ratios. Furthermore, among the three composite films, films with EZ show higher swelling. NH_2 groups in the structure of EZ interact with water molecules by hydrogen bonds and result in the higher swelling [50]. The barrier property of the films is measured by the MPR process at 40 °C and 85% relative humidity for 24 h as shown in Fig. 12b. The PET and POL/PET films had the MPR values of 4.25 $g\,m^{-2}\,d^{-1}$ and 3.65 $g\,m^{-2}\,d^{-1}$ MPR, respectively.

There is a reduction in the permeation of the films with EZ3/PET (2.02 $g\,m^{-2}\,d^{-1}$), PZ3/PET (2.22 $g\,m^{-2}\,d^{-1}$), and FZ3/PET (3.34 $g\,m^{-2}\,d^{-1}$), which shows the lowest permeation among the ratios of each Bzo group. Among the Bzo films, EZ3 shows the lowest permeation, which allows 47.5% higher permeation than PET. For EZ7/PET, PZ7/PET, and FZ10/PET, the values of MPR are 3.85 $g\,m^{-2}\,d^{-1}$, 6.48 $g\,m^{-2}\,d^{-1}$, and 5.54 $g\,m^{-2}\,d^{-1}$, respectively, which are greater than that of the POL/PET film (3.65 $g\,m^{-2}\,d^{-1}$), although this ratio provides the lowest swelling ratio. Here, the addition of Bzo to the POL improves the hydrophobic property of the composite film. A good composite can be obtained with the optimized addition ratio of Bzo to the POL, resulting in lower permeation. The higher ratio of Bzo to the POL causes phase separation among the polymers, leading to the higher permeation rate. Even though, the higher ratio Bzo to the POL leads to lower swelling.

In most cases, a catalyst is used for the Bzo to reduce the polymerization temperature. However, fragile materials are produced with the use of a catalyst [51]. To overcome this limitation, researchers aim to synthesize various new materials by grafting the imidazole on the core structure [44,52]. However, the composite epoxy and Bzo have the advantage of reducing the polymerization temperature of Bzo by using imidazole as a catalyst and as a liner for epoxy. Moreover, the present study has the benefit of a low-temperature fabrication. From different studies, it can be seen that polymer-based films polyvinyl alcohol allows the permeation rate of 4.2 $g\,m^{-2}\,d^{-1}$ [53]. The composite of cyclic olefin copolymer and Zr_6O_4 (OH) $_4$ (fumarate) $_6$ metal-organic framework film allowed 84% higher permeation compared with the PET [54]. The film of composite poly (styrene-b-2-vinyl pyridine) and MgO allows 68.8% higher permeation compared with poly (styrene-b-2-vinyl pyridine) film [55]. In the present study, EZ3/PET allows only 47.5% higher permeation than the PET, which is a significant improvement for a barrier film.

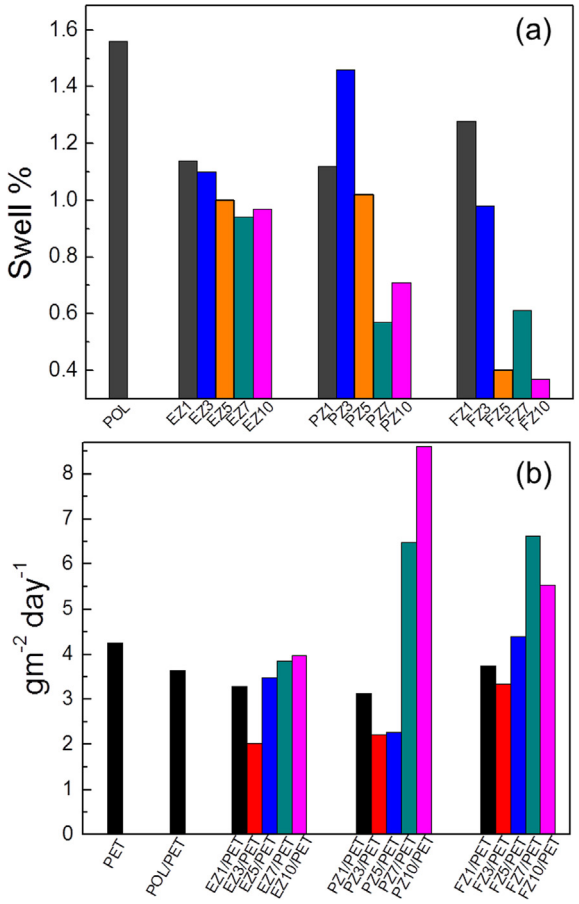

Fig. 12. Barrier abilities measurement (a) swell ratio, and (b) moisture permeation rate (MPR).

4. Conclusions

In conclusion, we synthesized three different benzoxazine monomers, EZ, PZ, and FZ, and an increased hydrophobic POL- poly Bzo composite was produced. Imidazole was used as a catalyst to reduce the polymerization temperatures of benzoxazine. Further, it was used as a cross-linker for epoxy and phenoxy. Films were fabricated from the solutions at low temperatures with an applicator. The composite films EZ1 and EZ3 on PET obtained excellent transmittance (approx. 90%). In both acidic and basic mediums, the stability of EZ composite films increased. The EZ3/PET film also exhibited the lowest moisture permeation rates ($2.02\,g\,m^{-2}\,d^{-1}$), which only allowed 47.5% higher permeation than a PET substrate. This new polymer composition of the barrier film and the facile fabrication process could be a potential candidate for printed organic electronic devices. In the future, multilayer films with polybenzoxazine compositions have been expected to achieve further reductions in permeation rates.

Acknowledgements

This work has supported by the National Research Foundation of Korea (NRF) grant funded by the Korea government (MSIT) (NRF-2018R1A1A3A04076752).

Appendix A. Supplementary material

Supplementary data to this article can be found online at https://doi.org/10.1016/j.eurpolymj.2019.04.039.

References

[1] K. Liu, T.T. Larsen-Olsen, Y. Lin, M. Beliatis, E. Bundgaard, M. Jorgensen, F.C. Krebs, X. Zhan, Roll-coating fabrication of flexible organic solar cells: comparison of fullerene and fullerene-free systems, J. Mater. Chem. A 4 (2016) 1044–1051, https://doi.org/10.1039/C5TA07357J.
[2] T. Wang, Y. Guo, P. Wan, X. Sun, H. Zhang, Z. Yua, Flexible transparent colorimetric wrist strap sensor, Nanoscale 9 (2017) 869–874, https://doi.org/10.1039/C6NR08265C.
[3] Y. Qu, C. Coburn, D. Fan, S.R. Forrest, Elimination of plasmon losses and enhanced light extraction of top-emitting organic light-emitting devices using a reflective subelectrode grid, ACS Photonics 4 (2017) 363–368, https://doi.org/10.1021/acsphotonics.6b00847.
[4] J.H. Seo, I. Hwang, H.D. Um, S. Lee, J. Park, H. Shin, T.H. Kwon, S.J. Kang, K. Seo, Cold isostatic-pressured silver nanowire electrodes for flexible organic solar cells via room-temperature processes, Adv. Mater. 29 (2017) 1–8, https://doi.org/10.1002/adma.201701479.
[5] M. Schaer, F. Nuesch, D. Berner, W. Leo, L. Zuppiroli, Water vapor and oxygen degradation mechanisms in organic light emitting diodes, Adv. Funct. Mater. 11 (2001) 116–121, https://doi.org/10.1002/16163028(200104)11:2<116::AID-ADFM116>3.0.CO;2-B.
[6] D. Yu, Y.Q. Yang, Z. Chen, Y. Tao, Y.F. Liu, Recent progress on thin-film encapsulation technologies for organic electronic devices, Opt. Commun. 362 (2016) 43–49, https://doi.org/10.1016/j.optcom.2015.08.021.
[7] J. Lewis, Material challenge for flexible organic devices, Mater. Today 9 (2006) 38–45, https://doi.org/10.1016/S1369-7021(06)71446-8.
[8] S. Seethamraju, P.C. Ramamurthy, G. Madras, Reactive interlayer based ultra-low moisture permeable membranes for organic photovoltaic encapsulation, Phys. Chem. Chem. Phys. 17 (2015) 23165–23172, https://doi.org/10.1039/C5CP04255K.
[9] G.N. Kopanati, P.C. Ramamurthy, G. Madras, TiO_2/EVOH based reactive interlayer in Surlyn for organic device encapsulation, Mater. Res. Express 3 (2016) 025302, https://doi.org/10.1088/2053-1591/3/2/025302.
[10] M. Jens, G. Patrick, B. Franz, H. Sami, W. Thomas, H.H. Johannes, W. Thomas, H. Peter, R. Thomas, K. Wolfgang, Al_2O_3/ZrO_2 Nanolaminates as ultrahigh gas-diffusion barriersa strategy for reliable encapsulation of organic electronics, Adv. Mater. 21 (2009) 1845–1849, https://doi.org/10.1002/adma.200803440.
[11] S. Gupta, S. Seethamraju, P.C. Ramamurthy, G. Madras, Polyvinylbutyral based hybrid organic/inorganic films as a moisture barrier material, Ind. Eng. Chem. Res. 52 (2013) 4383–4394, https://doi.org/10.1021/ie3022412.
[12] N. Frederik, D. Felix, K. Hannes, M. Lars, L. Karl, S. Aarti, R. Claudia, S. Uwe, M. Thomas, H. Christoph, A. Matthias, W.B. Johann, Atomic layer deposited TiOx/AlOx nanolaminates as moisture barriers for organic devices, Org, Electron. physics, Mater. Appl 38 (2016) 84–88, https://doi.org/10.1016/j.orgel.2016.07.037.
[13] Y. Jungheum, L. Sunghun, J. Yujeong, H. Lee, K. Jung-Dae, G.H. Lee, Reduction of defects in SiOx vapor permeation barriers on polymer substrates by introducing a sputtered interlayer, Jpn. J. Appl. Phys. 48 (2009) 0555031–0555035, https://doi.org/10.1143/JJAP.48.055503.
[14] A. Gupta, G.N. Parsons, Bond strain, chemical induction, and OH incorporation in low-temperature (350–100°C) plasma deposited silicon dioxide films, J. Vac. Sci. Technol., B 18 (2000) 1764–1769, https://doi.org/10.1116/1.591468.
[15] S. Logothetidis, A. Laskarakis, D. Georgiou1, S. Amberg-Schwab, U. Weber, K. Noller, M. Schmidt, E. Küçükpinar, W. Lohwasser, Ultra high barrier materials for encapsulation of flexible organic electronics, Eur. Phys. J. Appl. Phys. 51 (2011) 00618493, https://doi.org/10.1051/epjap/2010102.
[16] A.P. Roberts, B.M. Henry, A.P. Sutton, C.R.M. Grovenor, G.A.D. Briggs, T. Miyamoto, M. Kano, Y. Tsukahara, M. Yanaka, Gas permeation in silicon-oxide/polymer (SiOx/PET) barrier films: role of the oxide lattice, nano-defects and macro-defects, J. Membrance Sci. 208 (2002) 75–88, https://doi.org/10.1016/S0376-7388(02)00178-3.
[17] C.C. Chiang, D.S. Wuu, H.B. Lin, Y.P. Chen, T.N. Chen, Y.C. Lin, C.C. Wu, W.C. Chen, T.H. Jaw, R.H. Horng, Deposition and permeation properties of SiNx/parylene multilayers on polymeric substrates, Surf. Coat. Technol. 200 (2006) 5843–5848, https://doi.org/10.1016/j.surfcoat.2005.08.133.
[18] A. Hofrichter, P. Bulkin, B. Drévillon, Plasma treatment of polycarbonate for improved adhesion, J. Vac. Sci. Technol. A 20 (2002) 245, https://doi.org/10.1116/1.1430425.
[19] M. Keil, C.S. Rastomjee, A. Rajagopal, H. Sotobayashi, A.M. Bradshaw, C.L.A. Lamont, D. Gador, C. Buchberger, R. Fink, E. Umbach, Argon plasma-induced modifications at the surface of polycarbonate thin films, Appl. Surf. Sci. 125 (1998) 273–286, https://doi.org/10.1016/S0169-4332(97)00501-1.
[20] G.N. Kopanati, S. Seethamraju, P.C. Ramamurthy, G. Madras, Ionomer based blend as water vapor barrier materials for organic device encapsulation, ACS Appl. Mater. Interfaces 5 (2013) 4409–4416, https://doi.org/10.1021/am4007808.
[21] L.K. Massey, Permeability Properties of Plastics and Elastomers, third ed., William Andrew Publishing, NewYork, 2003.
[22] E.M. Petrie, Epoxy Adhesive Formulations, McGraw-Hill Companies, New York, 2006.
[23] S. Chang-Hoon, K. Yeun-Soo, M. Ki-Jeong, Phenoxy resin composition for transparent plastic substrate and transparent plastic substrate using the same. US Patent-0107248A1, 2014.
[24] H. Ishida, D.J. Allen, Physical and mechanical characterization of near-zero shrinkage polybenzoxazines, J. Polym. Sci. Part B: Polym. Phys. 34 (1996) 1019–1030, https://doi.org/10.1002/(SICI)1099-0488(19960430)34:6<1019::AID-POLB1>3.0.CO;2-T.

[25] N.N. Ghosh, B. Kiskan, Y. Yagci, Polybenzoxazines-new high performance thermosetting resins: synthesis and properties, Prog. Polym. Sci. 32 (2007) 1344–1391, https://doi.org/10.1016/j.progpolymsci.2007.07.002.
[26] M. Poortemana, A. Renauda, J. Escobara, L. Dumasa, L. Bonnaudb, P. Duboisb, M.G. Oliviera, Thermal curing of para-phenylenediamine benzoxazine for barrier coating applications on 1050 aluminum alloys, Prog. Org. Coat. 97 (2016) 99–109, https://doi.org/10.1016/j.porgcoat.2016.03.026.
[27] J. Escobar, M. Poorteman, L. Dumasa, L. Bonnaud, P. Dubois, M.G. Olivier, Thermal curing study of bisphenol A enzoxazine for barrier coating applications on 1050 aluminum alloy, Prog. Org. Coat. 79 (2015) 53–61, https://doi.org/10.1016/j.porgcoat.2014.11.004.
[28] A.S. Parveen, H. Kim, Synthesis and properties of main-chain polybenzoxazines based on bisphenol-S. Polym, Polym. Eng. Sci. 58 (10) (2017) 1–8, https://doi.org/10.1002/pen.24777.
[29] A.S. Parveen, P. Thirukumaran, M. Sarojadevi, Low dielectric materials from fluorinated polybenzoxazines, Polym. Adv. Technol. 25 (2014) 1538–1545, https://doi.org/10.1002/pat.3398.
[30] J.Y. Hyun, G. Cho, S.K. Chang, Adhesive Film. US Patent- 20130251989A1, 2013.
[31] S. Rimdusit, C. Jubsilp, S. Tiptipakorn, Alloys and Composites of Polybenzoxazines Properties and Applications, Springer, New York, 2013, pp. 47–56.
[32] A. Akhgari, F. Farahmand, G.H. Afrasiabi, F. Sadeghi, T. Vandamme, The effect of pectin on swelling and permeability characteristics of free films containing Eudragit RL and/or RS as a coating formulation aimed for colonic drug delivery, Daru 18 (2) (2010) 24–29 PMC3304378.
[33] Standard Practices for Evaluating the Resistance of Plastics to Chemical. ASTM D543-06, 2006.
[34] G.A.K.M.R. Bari, S. Park, A.S. Parveen, S. Lee, H. Kim, High barrier performance of the multilayer film based on epoxy and montmorillonite, Prog. Org. Coat. 126 (2019) 1–7, https://doi.org/10.1016/j.porgcoat.2018.10.017.
[35] T. Agag, T. Takeichi, Synthesis and characterization of novel benzoxazine monomers containing allyl groups and their high performance thermosets, Macromolecules 36 (2003) 6010–6017, https://doi.org/10.1021/ma021775q.
[36] L. Shengfang, Y. Shilin, Y. Jianying, B. Yu, Synthesis and characterization of new benzoxazine-based phenolic resins from renewable resources and the properties of their polymers, J. Appl. Polym. Sci. 122 (2011) 2843–2848, https://doi.org/10.1002/app.34342.
[37] P. Thirukumaran, A. Shakila, S. Muthusamy, Synthesis and characterization of novel bio-based benzoxazines from eugenol, RSC Adv. 4 (2014) 7959–7966, https://doi.org/10.1039/C3RA46582A.
[38] X. Wang, F. Chen, Y. Gu, Influence of electronic effects from bridging groups on synthetic reaction and thermally activated polymerization of bisphenol-based benzoxazines, J. Polym. Sci., Part A: Polym. Chem. 49 (2011) 1443–1452, https://doi.org/10.1002/pola.24566.
[39] S.P. Zhang, H.O. Song, Supramolecular graphene oxide-alkylamine hybrid materials: variation of dispersibility and improvement of thermal stability, New J. Chem. 36 (2012) 1733–1738, https://doi.org/10.1039/C2NJ40214A.
[40] E. Chiavaro, Differential Scanning Calorimetry, CRC Press, Taylor & Francis Group, NewYork, 2015.
[41] H. Wang, P. Zhao, H. Ling, Q. Ran, Y. Gu, Y, The effect of curing cycles on curing reactions and properties of a ternary system based on benzoxazine, epoxy resin, and imidazole, J. Appl. Polym. Sci. 127 (2012) 2169–2175, https://doi.org/10.1002/app.37778.
[42] S. Rimdusit, H. Ishida, Development of new class of electronic packaging materials based on ternary systems of benzoxazine, epoxy, and phenolic resins, Polymer 41 (2000) 7941–7949, https://doi.org/10.1016/S0032-3861(00)00164-6.
[43] A. Chernykh, T. Agag, H. Ishida, Novel benzoxazine monomer containing diacetylene linkage: an approach to benzoxazine thermosets with low polymerization temperature without added initiators or catalysts, Polymer 50 (2009) 3153–3157, https://doi.org/10.1016/j.polymer.2009.04.061.
[44] K. Kannan, S. Krishnan, M. Chavali, M. Alagar, Studies on thermal behavior of imidazole diamine based benzoxazines, J. Appl. Polym. Sci. 135 (2018) 46562, https://doi.org/10.1002/app.46562.
[45] Y. Wang, X. Niu, X. Xing, S. Wang, X. Jing, Curing behaviour and properties of a novel benzoxazine resin via catalysis of 2-phenyl-1,3,2-benzodioxaborole, React. Funct. Polym. 117 (2017) 60–69, https://doi.org/10.1016/j.reactfunctpolym.2017.06.004.
[46] H. Wang, Z. Rongqi, P. Yang, Y. Gu, A study on the chain propagation of benzoxazine, Polym. Chem. 7 (2016) 860–866, https://doi.org/10.1039/C5PY01397F.
[47] R. Grover, R. Srivastava, O. Rana, D.S. Mehta, M.N. Kamalasanan, New organic thin-film encapsulation for organic light emitting diodes, J. Encapsulation Adsorpt. Sci. 2011 (2011) 23–28, https://doi.org/10.4236/jeas.2011.12003.
[48] V. Nevissas, J.M. Widmaier, G.C. Meyer, Effect of crosslink density and interpenetrating polymer networks, J. Appl. Polym. Sci. 36 (1988) 1467–1473, https://doi.org/10.1002/app.1988.070360616.
[49] R. Ballestero, B.M. Sundaram, H.V. Tippur, M.L. Auad, Sequential graft-interpenetrating polymer networks based on polyurethane and acrylic/ester copolymers, eXPRESS Polymer Lett. 10 (2016) 204–215 http://hdl.handle.net/10415/4884.
[50] W.H. Koo, S.M. Jeong, S.H. Choi, H.K. Baik, Water vapor barrier properties of transparent SnO_2-SiO_x composite films on polymer substrate, J. Phys. Chem. B 180 (2004) 18884–18889, https://doi.org/10.1021/jp047617d.
[51] P. Yang, Y. Gu, A novel benzimidazole moiety containing benzoxazine: synthesis, polymerization, and thermal properties, J. Polym. Sci. A 50 (2012) 1261–1271, https://doi.org/10.1002/pola.25873.
[52] A. Hariharan, K. Srinivasan, C. Murthy, M. Alagar, A novel imidazole-core-based benzoxazine and its blends for high-performance applications, Ind. Eng. Chem. Res. 56 (2017) 9347–9354, https://doi.org/10.1021/acs.iecr.7b01816.
[53] S. Gupta, S. Sindhu, K.A. Varman, P.C. Ramamurthy, G. Madras, Hybrid nanocomposite films of polyvinyl alcohol and ZnO as interactive gas barrier layers for electronic device passivation, RSC Adv. 2 (2012) 11536–11543, https://doi.org/10.1039/C2RA21714G.
[54] Y.J. Bae, E.S. Cho, F. Qiu, D.T. Sun, T.E. Williams, J.J. Urban, W.L. Queen, Transparent metal-organic framework/polymer mixed matrix membranes as water vapor barriers, ACS Appl. Mater. Interfaces 8 (2016) 10098–10103, https://doi.org/10.1021/acsami.6b01299.
[55] E.S. Cho, C.M. Evans, E.C. Davidson, M.L. Hoarfrost, M.A. Modestino, Enhanced water vapor blocking in transparent hybrid polymer-nanocrystal films, ACS Macro Lett. 4 (2015) 70–74, https://doi.org/10.1021/mz500765y.